TiO_2 Stability Landscape: Polymorphism, Surface Energy, and Bound Water Energetics

Andrey A. Levchenko,[†] Guangshe Li,[‡] Juliana Boerio-Goates,[§] Brian F. Woodfield,[§] and Alexandra Navrotsky*,[†]

Thermochemistry Facility and NEAT ORU, University of California at Davis, Davis, California, Fujian Institute of the Research on the Structure of Matter, Chinese Academy of Sciences, P. R. China, and Brigham Young University, Provo, Utah

Received May 19, 2006. Revised Manuscript Received September 18, 2006

The energetics of pure-phase rutile nanorods and spherical anatase nanoparticles have been studied by high-temperature drop solution calorimetry in $3Na_2O{\cdot}4MoO_3$ solvent at 975 K and water adsorption calorimetry in a wide range of particle sizes (surface area) from 6 to 40 nm (5−270 m^2/g). The calorimetric surface enthalpies for rutile and anatase, calculated as 2.22 ± 0.07 and 0.74 ± 0.04 J/m^2, respectively, are in general agreement with Ranade et al.'s results (*Proc. Natl. Acad. Sci. U.S.A.*, **2002**, *99*, 6476), although their numerical values are somewhat different because of impurities and unaccounted bound water in the previous work. This study supports the energy crossovers previously proposed for the TiO_2 polymorphs. The energetics of water adsorption were measured using a commercial Calvet microcalorimeter coupled with a gas dosing system. This permitted the calculation of differential and integral enthalpies of water adsorption that characterize how tightly water binds to rutile and anatase surfaces and the calculation of adsorption entropies, which reflect the surface mobility of adsorbed water. The integral enthalpy of tightly bound water (relative to liquid H_2O standard state) is −18 kJ/mol for anatase and −40 kJ/mol for rutile. As seen previously for Al_2O_3, the TiO_2 polymorphs with higher surface energy bind water more tightly. The calculated entropy changes for the adsorption of water on TiO_2 are more negative than the entropy changes for the condensation of gaseous water to hexagonal ice. This finding suggests highly restricted mobility of molecules adsorbed at initial stages of adsorption (low coverage) and, possibly, dissociative adsorption on both rutile and anatase surfaces. However, nanoparticles contain both tightly bound water and loosely bound water. The latter is characterized by energetics of bulk water. The stabilizing water contribution to the overall energy of the system makes the hydrated nanophase samples more stable. The recommended transformation enthalpy for bulk anatase to bulk rutile is −1.7 ± 0.9 kJ/mol.

Introduction

Rutile and anatase are the two most abundant and widely used polymorphs of TiO_2, whose current and promising applications include paint, catalysts and photocatalysts, solar cells, and ductile ceramics.[1,2] Although both polymorphs crystallize in a tetragonal structure, they have different symmetry and properties.[2] For example, anatase is catalytically more efficient than rutile.[3]

Rutile is the thermodynamically stable phase in coarse materials, but anatase is common in nanosized samples.[4−7] Thermodynamic properties of nanosized materials differ from those of the bulk by a surface energy term, whose contribution increases as the surface area grows with decreasing particle size. Recently, Ranade et al.[8] established by direct calorimetric measurements of enthalpy of solution into a molten oxide solvent that the surface energy of rutile, anatase, and brookite decreases in that order, whereas for bulk samples, the metastability increases in the same sequence. This competition between polymorphism and surface energy leads to a crossover in thermodynamic stability at the nanoscale level, with brookite and anatase each having a range of particle size in which they are thermodynamically stable as long as coarsening cannot occur. The generality of such crossovers in stability at the nanoscale level, found in many systems, has been discussed by Navrotsky.[9]

* Corresponding author. E-mail: anavrotsky@ucdavis.edu.
[†] University of California at Davis.
[‡] Chinese Academy of Sciences.
[§] Brigham Young University.

(1) Diebold, U. *Appl. Phys. A: Mater. Sci. Process.* **2003**, *76* (5), 681−687.
(2) Wells, A. F. *Structural Inorganic Chemistry*, 4th ed.; Clarendon Press: Oxford, 1975; pp xxiii and 1095, [4] leaves of plates.
(3) Nagaveni, K.; Sivalingam, G.; Hedge, M. S.; Madras, G. *Appl. Catal., B* **2004**, *48* (2), 83−93. Nagaveni, K.; Sivalingam, G.; Hegde, M. S.; Madras, G. *Environ. Sci. Technol.* **2004**, *38* (5), 1600−1604.
(4) Zhang, H. Z.; Banfield, J. F. *Am. Mineral.* **1999**, *84* (4), 528−535. Zhang, H. Z.; Banfield, J. F. *J. Mater. Res.* **2000**, *15* (2), 437−448. Zhang, H. Z.; Banfield, J. F. *Chem. Mater.* **2002**, *14* (10), 4145−4154. Zhang, Q.; Gao, L. *Langmuir* **2003**, *19*, 967−971. Zhang, Q. H.; Gao, L.; Guo, J. K. *Nanostruct. Mater.* **1999**, *11* (8), 1293−1300.
(5) Zhang, H. Z.; Banfield, J. F. *J. Phys. Chem. B* **2000**, *104* (15), 3481−3487.
(6) Zhang, H. Z.; Finnegan, M.; Banfield, J. F. *Nano Lett.* **2001**, *1* (2), 81−85.
(7) Zhang, H. Z.; Penn, R. L.; Hamers, R. J.; Banfield, J. F. *J. Phys. Chem. B* **1999**, *103* (22), 4656−4662.
(8) Ranade, M. R.; Navrotsky, A.; Zhang, H. Z.; Banfield, J. F.; Elder, S. H.; Zaban, A.; Borse, P. H.; Kulkarni, S. K.; Doran, G. S.; Whitfield, H. J. *Proc. Natl. Acad.Sci. U.S.A.* **2002**, *99*, 6476−6481.
(9) Navrotsky, A. *Proc. Natl. Acad.Sci. U.S.A.* **2004**, *101* (33), 12096−12101. Navrotsky, A. *Abstr. Pap. Am. Chem. Soc.* **2003**, *225*, U939−U939.

10.1021/cm061183c CCC: $33.50
Published on Web 11/23/2006

However, the work of Ranade et al.[8] was based on a relatively small number of samples obtained from several different sources and prepared by various methods. Because nanophase samples almost always contain adsorbed water, a correction to the calorimetric data for this water must be made. Ranade et al.[8] approximated this correction by using the heat content of water with liquid water at 298 K as the reference state. This correction is thus approximate in that it assumes the H_2O adsorbed on nanoparticle surfaces has the thermodynamic properties of pure liquid water.

The issue of surface water stabilizing nanoparticles or driving transformations between polymorphs has been intensively discussed in the literature.[10−14] This is because water bound to the surface decreases the free energy of the system and therefore affects the overall stability landscape. Early work by McHale et al.[12,13] on a crossover in energetics of nanophase Al_2O_3 showed that corundum (α-Al_2O_3) has a large number of highly energetic sites for strong water adsorption in comparison with γ-Al_2O_3, which is lower in energy than α-Al_2O_3 at the nanoscale. These findings imply synergy between phase stability, surface energy, and water energetics for oxide nanoparticles. Kinetic studies by Li et al.[14] on a newly synthesized series of anatase nanoparticles demonstrated the role of surface water as a kinetic barrier that governs the anatase-to-rutile transformation. Although the overall binding of water on TiO_2 is almost certainly weaker than on Al_2O_3, we anticipate that the bound water on TiO_2 is nevertheless essential to the stabilization of very small nanoparticles of TiO_2, especially those synthesized under hydrothermal conditions.

The goal of the present study is to use a large set of similarly synthesized samples of nanophase anatase and rutile to obtain the enthalpies and entropies of water adsorption, the surface energies (referring to both dry and hydrated surfaces), and the energetics of polymorphism. The calorimetric study of water adsorption is the first of its kind for TiO_2, whereas the measurements of surface and transformation enthalpies represent a refinement of the data of Ranade et al.[8]

Experimental Section

Synthesis. Phase pure rutile nanorods were synthesized using a hydrothermal technique.[15] A 0.67 M $TiOCl_2$ solution was prepared by slowly adding $TiCl_4$ to distilled water at room temperature. Thirty milliliters of this solution was moved to Teflon-lined autoclaves to allow reactions at selected temperatures for 2 h. A modified sol−gel method was also employed to obtain high-quality spherical anatase nanoparticles.[14] $TiCl_4$ was added slowly to ice-cooled ethanol while stirring. The sol thus formed was allowed to remain in air for several hours and was then baked at 358 K until it became white powder. The white powder was determined by X-ray diffraction (XRD) to be pure anatase 7 nm in size. The procedures are simililar to those reported previously, and the majority of the samples used in the study are from the same batches as those in the references.[14,15]

Samples with extremely low impurities were achieved by a large number of washings of the reaction samples using centrifuges at room temperature. The resulting white powder was dried in an oven at 353 K in air and used for further analysis. The only impurities found were carbon and chlorine, but both were only at the parts per million level.

Characterization. XRD patterns were collected using a Scintag PAD V diffractometer (Cu Kα, 45 kV, 40 mA, $\theta-2\theta$ goniometer geometry) with a step size of 0.02° and collection time of 10 s/step (without an internal standard). XRD verified that the samples were single-phase nanophase anatase and rutile. The actual XRD patterns and TEM images for rutile and anatase samples used in the study have been previously analyzed and published in a series of papers[14,15] and are therefore not reported here. The average particle sizes were calculated from the most intense peaks, (110) for rutile and (101) for anatase, using the Scherrer formula.[15] The specific surface areas of the materials were obtained according to the Brunauer−Emmett−Teller (BET) equation[16] from N_2 adsorption at 77 K in a relative pressure range $p/p^0 = 0.05-0.3$ (p^0 = saturation pressure) using a Micromeritics ASAP 2020 surface area and porosity analyzer. For BET measurements, each sample was degassed at 373 K for at least 10 h after a stable static vacuum of 3×10^{-3} Torr was reached. Water contents of samples introduced into the calorimeter were determined by thermogravimetric analyses (TGA) on 20−30 mg pellets using a Netzsch STA 449 system. The heating rate was 10 K/min to 1373 K, and dry O_2 was used as a carrier gas to mimic calorimetric conditions (see below). Buoyancy corrections were made by recording empty crucible baselines for all runs. The molar compositions (formula weights) were normalized to obtain 1 mole of TiO_2 and w moles of water. Gases evolved during thermal analysis were analyzed by a Bruker Equinox 55 FTIR spectrometer, which is directly coupled with the TG/DSC by a heated transfer line kept at 423 K. FTIR spectra of evolved gases were collected from 400 to 4000 cm^{-1} at a resolution of 4 cm^{-1}. A baseline correction was made before each run.

Drop Solution and Water Adsorption Calorimetry. All moisture-sensitive nanocrystalline samples were handled in an Ar-filled glovebox (O_2 and H_2O levels below 1 ppm). Drop solution enthalpies in $3Na_2O{\cdot}4MoO_3$ solvent at 975 K were measured using a custom-built Calvet twin microcalorimeter. Oxidizing conditions were maintained by flushing O_2 through the glassware at ~80 mL/min and bubbling through the solvent at ~5 mL/min. This also assisted in removal of evolved water and agitated the solvent to aid dissolution. The samples were pressed into pellets (~5 mg) inside the glovebox, weighed, and stored in glass vials. After calorimeter baseline stability was achieved, the pellet from the glass vial was dropped into the calorimeter. The total time the pellet was exposed to air was less than 5 s. The calibration factors for the calorimeter ($J/\mu V$) were obtained by dropping 5 mg pellets of alumina (Aldrich, 99.99%) stabilized in the corundum phase by heating overnight at 1773 K. The overall methodology is now standard and has been reported previously.[17] Enthalpies of water adsorption were recorded using a Setaram Calvet-type DSC 111

(10) Zhang, H. Z.; Gilbert, B.; Huang, F.; Banfield, J. F. *Nature* **2003**, *424* (6952), 1025−1029.
(11) Zhang, H. Z.; Huang, F.; Gilbert, B.; Banfield, J. F. *J. Phys. Chem. B* **2003**, *107* (47), 13051−13060.
(12) McHale, J. M.; Auroux, A.; Perrotta, A. J.; Navrotsky, A. *Science* **1997**, *277* (5327), 788−791.
(13) McHale, J. M.; Navrotsky, A.; Perrotta, A. J. *J. Phys. Chem. B* **1997**, *101* (4), 603−613.
(14) Li, G. S.; Li, L. P.; Boerio-Goates, J.; Woodfield, B. F. *J. Am. Chem. Soc.* **2005**, *127* (24), 8659−8666.
(15) Li, G. S.; Li, L. P.; Boerio-Goates, J.; Woodfield, B. F. *J. Mater. Res.* **2003**, *18* (11), 2664−2669.
(16) Brunauer, S.; Emmett, P. H.; Teller, E. *J. Am. Chem. Soc.* **1938**, *60*, 308. Sing, K. S. W.; Everett, D. H.; Haul, R. A. W.; Moscou, L.; Pierotti, R. A.; Rouquerol, J.; Siemieniewska, T. *Pure Appl. Chem.* **1985**, *57* (4), 603−619.
(17) Navrotsky, A. *Phys. Chem. Miner.* **1977**, *2* (1−2), 89−104. Navrotsky, A.; Rapp, R. P.; Smelik, E.; Burnley, P.; Circone, S.; Chai, L.; Bose, K. *Am. Mineral.* **1994**, *79* (11−12), 1099−1109.

Table 1. Sample Characterization and Thermochemical Data for Rutile and Anatase

sample	H_2O content *w*, per mole of TiO_2	surface area, m^2/g (m^2/mol)	particle size from BET (XRD), nm	ΔH_{ds}, J/g (no. of drops)	ΔH_{ds} uncorrected, kJ/mol of TiO_2	water correction, kJ/mol	ΔH_{ds} corrected, kJ/mol	ΔH_{tr}, kJ/mol
rutile (bulk)				741.3 ± 11[a] (12)	58.99 ± 0.80		58.99 ± 0.80	0.00 ± 0.80
rutile (r1)	0.350	104 (8307)	13 (7.1)	797.2 ± 12.4 (8)	76.01 ± 0.99	5.11	44.61 ± 0.99	18.04 ± 1.22
rutile (r2)	0.143	89 (7101)	16 (9.3)	681.7 ± 12.9 (9)	88.19 ± 1.03	2.18	46.36 ± 1.03	15.75 ± 1.26
rutile (r3)	0.185	60 (4785)	24 (13.2)	740.6 ± 9.1 (8)	63.00 ± 0.73	2.80	48.88 ± 0.73	9.83 ± 1.02
rutile (r4)	0.058	35 (2796)	41 (18.1)	681.7 ± 15.4 (9)	62.74 ± 1.23	0.90	51.19 ± 1.23	6.19 ± 1.43
rutile (r5)	0.045	20 (1598)	71 (22.6)	730.4 ± 8.3 (8)	57.10± 0.66	2.18	55.84 ± 0.66	3.85 ± 1.12
rutile (r6)	0.004	6 (479)	200 (33.6)	711.5 ± 5.4 (8)	145.95 ± 0.43	0.07	56.59 ± 0.43	2.61 ± 1.00
rutile (r11)	0.334	105 (8395)	14 (7.3)	781.0 ± 6.2 (9)	82.93 ± 0.50	4.90	44.06 ± 0.50	18.62 ± 1.03
rutile (r12)	0.181	66 (5272)	22 (9.2)	756.3 ± 9.3 (8)	65.90 ± 0.74	2.74	50.43 ± 0.74	10.88 ± 1.17
rutile (r13)	0.061	35 (2796)	41 (13)	705.1 ± 11.2 (8)	56.46 ± 0.89	0.95	52.88 ± 0.89	7.34 ± 1.27
rutile (r14)	0.013	21 (1693)	67 (17.7)	694.7 ± 8.1 (8)	72.03 ± 0.65	0.21	54.74 ± 0.65	4.67 ± 1.11
rutile (r15)	0.063	17 (1358)	84 (21.8)	795.7 ± 11.2 (8)	72.43 ± 0.80	0.98	54.80 ± 0.89	4.39 ± 1.20
rutile (r16)	0.054	5 (399)	286 (32.9)	741.8 ± 9.9 (8)	68.69 ± 0.72	0.84	58.32 ± 0.79	0.83 ± 1.15
rutile (r31)	0.037	29 (2277)	50 (13.4)	711.7 ± 10.1 (8)	78.25 ± 0.81	0.58	54.77 ± 0.81	5.22 ± 1.21
rutile (r32)	0.086	27 (2125)	54 (13.9)	735.0 ± 8.3 (7)	54.29 ± 0.66	1.33	53.92 ± 0.66	6.00 ± 1.122
rutile (r33)	0.001	21 (1677)	68 (14.8)	719.3 ± 11.9 (7)	59.84 ± 0.80	0.02	53.85 ± 0.63	6.06 ± 1.20
rutile (r34)	0.009	19 (1518)	75 (17.5)	739.5 ± 8.3 (8)	58.17 ± 0.64	0.14	56.28 ± 0.66	3.41 ± 1.10
rutile (r35)	0.004	9 (743)	154 (22.8)	701.5 ± 10.1 (7)	59.56 ± 0.81	0.07	55.79 ± 0.81	3.34 ± 1.21
rutile (r36)	0.013	6 (479)	238 (33.4)	726.8 ± 9.9 (7)	57.38 ± 0.56	0.21	57.12 ± 0.79	2.00 ± 1.06
anatase (a0)	0.49	270 (21567)	6 (7)	891.8 ± 15.0 (10)	71.23 ± 1.20	13.6	41.28 ± 1.20	17.70 ± 1.40
anatase (a1)	0.46	257 (20529)	6 (8.1)	898.0 ± 9.0 (7)	71.73 ± 0.72	13.6	43.21 ± 0.72	15.77 ± 1.02
anatase (a2)	0.27	218 (17414)	7 (9.3)	785.4 ± 8.6 (7)	62.74 ± 0.69	9.3	44.60 ± 0.69	14.38 ± 1.00
anatase (a3)	0.13	114 (9106)	14 (13.0)	753.9 ± 11.1 (8)	60.22 ± 0.88	8.9	50.97 ± 0.88	8.01 ± 1.14
anatase (a4)	0.08	89 (7101)	18 (16.8)	735.9 ± 8.6 (9)	58.79 ± 0.69	6.5	53.13 ± 0.69	5.85 ± 1.00
anatase (a5)	0.07	59 (4697)	27 (20.9)	748.2 ± 8.0 (9)	59.77 ± 0.64	8.8	55.02 ± 0.64	3.96 ± 0.96
anatase (a6)	0.04	37 (2956)	43 (28.9)	734.3 ± 9.8 (9)	58.65 ± 0.78	9.0	55.60 ± 0.78	3.38 ± 1.06
anatase (a11)	0.41	245 (19570)	6 (7.8)	881.0 ± 7.8 (9)	70.37 ± 0.98	12.7	44.63 ± 0.98	14.35 ± 1.22
anatase (a12)	0.27	207 (16535)	8 (9.1)	777.1 ± 11.7 (8)	62.08 ± 0.93	9.7	44.15 ± 0.93	14.83 ± 1.18
anatase (a13)	0.15	127 (10145)	12 (12.4)	736.7 ± 12.5 (8)	58.84 ± 1.00	8.6	48.75 ± 1.00	10.23 ± 1.23
anatase (a14)	0.08	80 (6382)	20 (17.1)	739.8 ± 12.0 (7)	59.10 ± 0.96	7.7	53.29 ± 0.96	5.69 ± 1.20
anatase (a15)	0.07	57 (4529)	28 (20.8)	731.1 ± 5.4 (7)	58.47 ± 0.43	9.0	53.80 ± 0.43	5.18 ± 0.84
anatase (a16)	0.06	44 (3515)	36 (28.2)	746.0 ± 9.2 (7)	59.59 ± 0.74	9.9	55.70 ± 0.74	3.28 ± 1.03
anatase (a31)	0.13	128 (10224)	12 (12.9)	721.9 ± 8.4 (8)	57.66 ± 0.67	7.6	48.44 ± 0.67	10.54 ± 0.98
anatase (a32)	0.12	118 (9426)	13 (13.3)	731.1 ± 6.8 (8)	58.40 ± 0.54	8.1	50.19 ± 0.54	8.79 ± 0.90
anatase (a34)	0.06	61 (4905)	26 (20.1)	739.5 ± 8.3 (8)	58.54 ± 0.69	8.6	52.91 ± 0.66	6.39 ± 0.98
anatase (a35)	0.09	78 (6215)	20 (17.0)	732.9 ± 8.6 (8)	59.07 ± 0.66	7.7	54.06 ± 0.69	5.24 ± 1.00

[a] The uncertainty is two standard deviations of the mean.

calorimeter coupled with the Micromeritics ASAP 2010 gas adsorption system used for precision gaseous water dosing and volumetric detection of adsorbed amounts as described before.[18] Each sample was degassed at 373 K for at least 3 days under a static vacuum of $<1 \times 10^{-5}$ Torr before water adsorption calorimetry. The TGA revealed that an average of 1.39 H_2O/nm^2 remained on the surface after degassing. This calorimetric measurement is very time consuming (each experiment takes 3−5 days), and therefore, water adsorption experiments were done on selected samples only.

Results and Discussion

Sample Characterization and Water Contents. We have prepared a large suite of well-characterized samples to evaluate the energetics of nanophase TiO_2 formation. Indeed, compared to the data of Ranade et al.,[8] our surface areas for pure phases span a wider range, from 37 to 270 m^2/g for anatase and from 5 to 105 m^2/g for rutile. Simple calculations based on a geometrical model of spherical particles yield particle sizes from 6 to 43 nm for anatase and from 13 to 286 nm for rutile, assuming densities equal to 3.893 and 4.25 g/cm^3, respectively (Table 1). Taking into account the simplicity of the model and nonspherical shape of rutile particles, sizes obtained by BET and XRD correlate well for particles <20 nm. Deviations can be explained by two important assumptions that contribute significantly to the error. First, we assume that the nanoparticles are spheres with smooth surfaces. Second, the calculation assumes that each particle is a single crystal. It is likely that particles >20 nm are polycrystalline, with crystallographic domain size smaller than particle size. This is in agreement with TEM observations of aggregation for anatase nanospheres.[6] A direct comparison between particle sizes obtained by BET and XRD requires the knowledge of particle shape as a function of size. Because of these complications and to be consistent with earlier work, we interpret energetics of nanophase TiO_2 in terms of surface areas calculated from BET experiments rather than the particle size.

Using both surface area and water content as variables, we separate the energetics of water adsorption from those of surface area increase. The TGA curves for anatase and rutile samples (Figure 1) show mass loss over a large temperature range, indicating a variety of bonding environments for the adsorbed water. It has been recognized that surface hydration cannot be removed completely from nanoparticles without causing coarsening.[10,14] Our attempts to dehydrate samples with the smallest particle sizes by heating in a vacuum above 373 K resulted in a surface area decrease (coarsening).

The evolved gas analyses (see insert in Figure 1) confirm that the only component associated with the mass loss is

(18) Ushakov, S. V.; Navrotsky, A. *Appl. Phys. Lett.* **2005**, *87* (16).

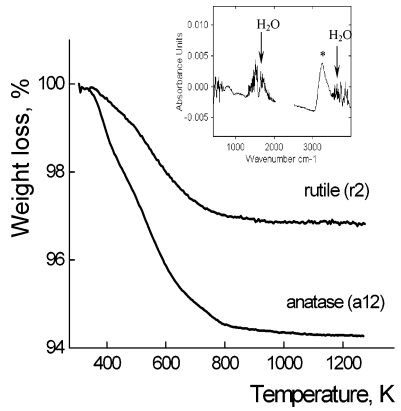

Figure 1. Typical TGA scans. Enclosed is an evolved gas FTIR spectrum. Asterisk represents a background water peak.

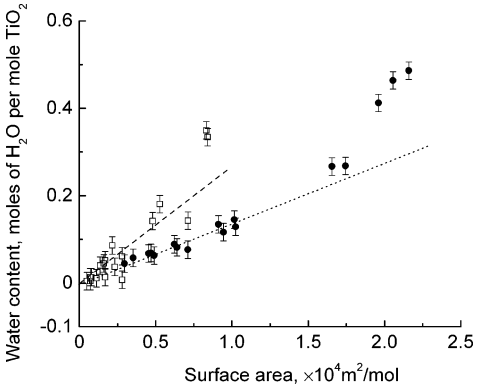

Figure 2. Water contents per mole of TiO_2 vs specific surface area: ●, anatase; □, rutile.

water, as indicated by many characteristic water bands. Together with TGA, the evolved gas FTIR confirms that water desorbs over a wide range of temperature, implying that some of the water is tightly bonded. This is in agreement with results obtained by Li et al.[14] using solid-state FTIR on 7.7 nm anatase nanospheres, which indicated 75% of water being in strong adsorption centers.

Water content as a function of surface area is depicted in Figure 2. It clearly shows two regimes for nanophase anatase. The H_2O contents for small-surface-area anatase (<130 m^2/g or 10300 m^2/mol) lie on a line with a constant slope, reflecting the same water coverage (the same number of water molecules per unit of surface area). Very small particles have higher water contents, as indicated by deviations from the line drawn through the lower surface area data. Rutile nanoparticles have a linear dependence of H_2O content on surface area, though with larger scatter and higher water coverage compared to anatase in the same surface-area range. The higher water coverage for rutile reflects a higher surface energy, as we will show later.

Water Adsorption Calorimetry. Because the water in TiO_2 is evolved at a much lower temperature than the water in Al_2O_3,[12] we expect less exothermic energetics of tightly bound water. Comprehensive studies of the energetics of water interaction with TiO_2 surfaces are scarce.[19] Previous experimental studies of water energetics on TiO_2 using temperature-programmed desorption[20,21] in water focused on particular crystallographic planes for rutile. The studies of TiO_2 immersion in water[22,23] lack the detailed information on water adsorption heats as a function of the water amount on the surface. In this study, water is dosed in tiny portions and adsorption heats are directly measured as a function of the water coverage.

The water adsorption reaction, H_2O (gas, 298 K) → H_2O (adsorbed, 298K), is spontaneous and results in a decrease in the system free energy. Because the condensed phase is more ordered, adsorption entropy decreases too, implying an exothermic heat effect according to a well-known relationship (all subscripts throughout the text relate to adsorption or to the adsorbed state)

$$\Delta_a G = \Delta_a H - T\Delta_a S \tag{1}$$

As shown by Hill,[24] the partial molar enthalpy of adsorption $\Delta_a\dot{h} = -[\partial Q/\partial n_a]_{T,m}$ (where Q, T, and m are heat effect, temperature, and mass, respectively) relates to the partial molar entropy of the adsorbate $\dot{s}_a$ as follows

$$\Delta_a\dot{h} = T(\dot{s}_a - s^g) = T\Delta_a\dot{s} \tag{2}$$

The entropies relative to liquid water and ice provide additional insights into adsorption layer order and molecular motion. Therefore, we calculate those quantities on the basis of experimental adsorption isotherms and enthalpies of adsorption.

The entropy of an ideal gas s^g is defined relative to the entropy under standard conditions $s^{0,g}$ by[25]

$$s^g = s^{0,g} - R\ln\frac{p}{p^0} \tag{3}$$

Therefore, the standard state partial molar entropy of adsorption (i.e., relative to gaseous water under standard pressure) can be written as

$$\Delta_a\dot{s}^0 = \dot{s}_a - s^{0,g} = \frac{\Delta_a\dot{h}}{T} - R\ln\frac{p}{p^0} \tag{4}$$

Equation 4 implies that

$$\dot{s}_a = \Delta_a\dot{s}^0 + s^{0,g} = \frac{\Delta_a\dot{h}}{T} - R\ln\frac{p}{p^0} + s^{0,g} \tag{5}$$

The entropy can also be expressed (see Appendix) relative to liquid water in equilibrium with its vapor ($p^{0,l}$ is the saturation pressure at 298 K)

(19) Morishige, K.; Tanabe, K.; Kita, H. *J. Res. Inst. Catal., Hokkaido Univ.* **1975**, *23* (2), 139−143.

(20) Brinkley, D.; Dietrich, M.; Engel, T.; Farrall, P.; Gantner, G.; Schafer, A.; Szuchmacher, A. *Surf. Sci.* **1998**, *395* (2−3), 292−306. Henderson, M. A. *Surf. Sci.* **1996**, *355* (1−3), 151−166.

(21) Hugenschmidt, M. B.; Gamble, L.; Campbell, C. T. *Surf. Sci.* **1994**, *302* (3), 329−340.

(22) Egashira, M.; Kawasumi, S.; Kagawa, S.; Seiyama, T. *Bull. Chem. Soc. Jpn.* **1978**, *51* (11), 3144−3149. Siriwardane, R. V.; Wightman, J. P. *J. Colloid Interface Sci.* **1983**, *94* (2), 502−513.

(23) Nagao, M.; Yunoki, K.; Muraishi, H.; Morimoto, T. *J. Phys. Chem.* **1978**, *82* (9), 1032−1035.

(24) Hill, T. L. *J. Chem. Phys.* **1950**, *18* (3), 246.

(25) Rouquerol, F.; Rouquerol, J.; Sing, K. S. W. *Adsorption by Powders and Porous Solids: Principles, Methodology, and Applications*; Academic Press: San Diego, 1999; pp xvi and 467.

$$\dot{s}_a - s^l = \frac{\Delta_a \dot{h}}{T} - R \ln\frac{p}{p^{0,l}} + \Delta_{evp} s^0 \quad (6)$$

In this case, $\Delta_{evp}s^0$ is the entropy change due to evaporation at 298 K and normal pressure.

It is interesting to compare the differential entropy of strongly bound water with that of hexagonal ice. The entropy of hexagonal ice at 273 K (38.1 J K^{-1} mol^{-1})[26] can be estimated through integration of ice heat capacity c_p^i extrapolated to 298 K. Boerio-Goates et al.[27] have estimated the heat capacity of hexagonal ice above 273 K. That estimate gives rise to an entropy (including the residual zero point entropy) of 44.77 J K^{-1} mol^{-1} at 298 K and an entropy increment of 3.4 J K^{-1} mol^{-1} for the 273−298 K interval.

Therefore, the differential entropy relative to hexagonal ice can be obtained through (see Appendix)

$$\Delta_a \dot{s}^s = \dot{s}_a - s^i = \frac{\Delta_a \dot{h}}{T} - R \ln\frac{p}{p^{0,i}} + \Delta_{evp} s^{0,l} + \frac{\Delta_m h}{T} - \int_{273}^{298} \frac{c_p^l}{T} dT + \int_{273}^{298} c_p^i \frac{dT}{T} \quad (7)$$

where $\Delta_{evp}s^{0,l}$ is the entropy change due to evaporation at 298 K and saturation pressure, $\Delta_m h$ is the ice melting enthalpy at 273 K, and c_p^l is the heat capacity of water.

In our adsorption experiments, the adsorption system is open, as infinitesimal amounts of water δn are admitted into the calorimeter. The general expression for the integral adsorption enthalpy (entropy) has terms related to the work of gas compression and spreading pressure.[25,28] Moreover, the partial molar enthalpy and entropy of adsorption are not full differentials and, hence, integral enthalpy and entropy cannot be derived by integration of their derivatives. As a result, another approach is adopted in the literature[28] to calculate integral quantities from partial molar enthalpies and entropies using adsorption isotherms. Using the second law of thermodynamics, we can write the entropy change of the system dS as[28]

$$dS = -\frac{Q}{T} + s^g\, dn \quad (8)$$

The entropy change can be expressed by the sum of two contributions corresponding to entropy changes of the adsorbed material $dS_a = d(s_a n_a)$ and gas $dS^g = d(s^g n^g)$. Using definitions of partial molar entropies, the system entropy change should read

$$dS = dS_a + dS^g = n_a\, ds_a + s_a\, dn_a + n^g\, ds^g + s^g\, dn^g \quad (9)$$

From eqs 8 and 9, one derives

$$-\frac{\delta Q}{T} = (s_a - s^g)\, dn_a + n_a\, ds_a + n^g\, ds^g \quad (10)$$

By adding and subtracting $n_a\, ds^g$ in eq 10, we arrive at the equation that contains the full differential of adsorption (the first right-hand term)[28]

$$-\frac{\delta Q}{T} = d[n_a(s_a - s^g)] + (n_a + n^g)\, ds^g \quad (11)$$

The differential entropy for the ideal gas is given by[26]

$$ds^g = -R\, d\left(\ln\frac{p}{p^0}\right) \quad (12)$$

where R is the gas constant, p is the gas pressure, and p^0 is the normal gas pressure.

Using eq 10, we can integrate eq 9 from 0 to n_a to give the following equation

$$\int_0^{n^a} -\frac{\delta Q}{T} = \int_0^{n^a} d[n_a(s_a - s^g)] - R\int_0^p n_a d\left(\ln\frac{p}{p^0}\right) - R\int_0^p n^g\, d\left(\ln\frac{p}{p^0}\right) \quad (13)$$

In the case of twin design of a Calvet calorimeter, the last term in eq 11 is zero because the corresponding heat affect, measured in both cells, cancels out. Therefore, the general equation for the integral molar entropy of adsorption includes the integral related to spreading pressure through[28,29]

$$\Delta_a s = -\frac{Q}{Tn_a} + \frac{R}{n_a}\int_0^p n_a\, d\ln\frac{p}{p^0} \quad (14)$$

where Q is the integral heat effect measured by the calorimeter.

Equation 12 reflects the fact that the adsorption experiment is carried out at increasing water vapor pressure. Generally, the last right-hand-side term in eq 12 cannot be neglected. However, for our experiments, this term is very small (on the order of 1×10^{-2} J mol^{-1} K^{-1}) compared to the first one, because calculation of the adsorption enthalpy for strongly bound water (see below) is done in a low-pressure range. Therefore, the measured heat effect δQ upon dosing of small amounts of gaseous water δn_a can be used to calculate the integral entropy as

$$\Delta_a s \approx -\frac{Q}{Tn_a} = \frac{\Delta_a h}{T} \quad (15)$$

The differential and integral heats of water adsorption are shown in Figure 3. As indicated by the differential heats of adsorption, the first 0.5 H_2O/nm^2 adsorbed on nanophase rutile yields adsorption enthalpies more negative than −120 kJ/mol. In contrast, only the first 0.25 H_2O/nm^2 adsorbed to nanophase anatase result in similar values, implying a greater number of highly energetic adsorption sites for rutile. We call water "strongly bound" water before the differential adsorption enthalpy reaches the condensation enthalpy of −44 kJ/mol at room temperature. The water remaining on the surface (an average coverage of 1.39 H_2O/nm^2), obtained by weight loss experiments after degassing, was accounted for by linear extrapolation of the integral enthalpy data below 1.5 H_2O/nm^2 to zero coverage and adjusted by adding average values of 0.30 and 0.17 J/m^2 to each data point for

(26) Ott, J. B.; Boerio-Goates, J. *Chemical Thermodynamics: Principles and Applications*; Academic Press: London, 2000; pp xxiii and 664.
(27) Boerio-Goates, J.; Li, G. S.; Li, L. P.; Walker, T. F.; Parry, T.; Woodfield, B. F. *Nano Lett.* **2006**, *6* (4), 750−754.
(28) Cardona-Martinez, N.; Dumesic, J. A. *Adv. Catal.* **1992**, *38*, 149.
(29) Rouquerol, F.; Rouquerol, J.; Dellagatta, G.; Letoquart, C. *Thermochim. Acta* **1980**, *39* (2), 151−158.

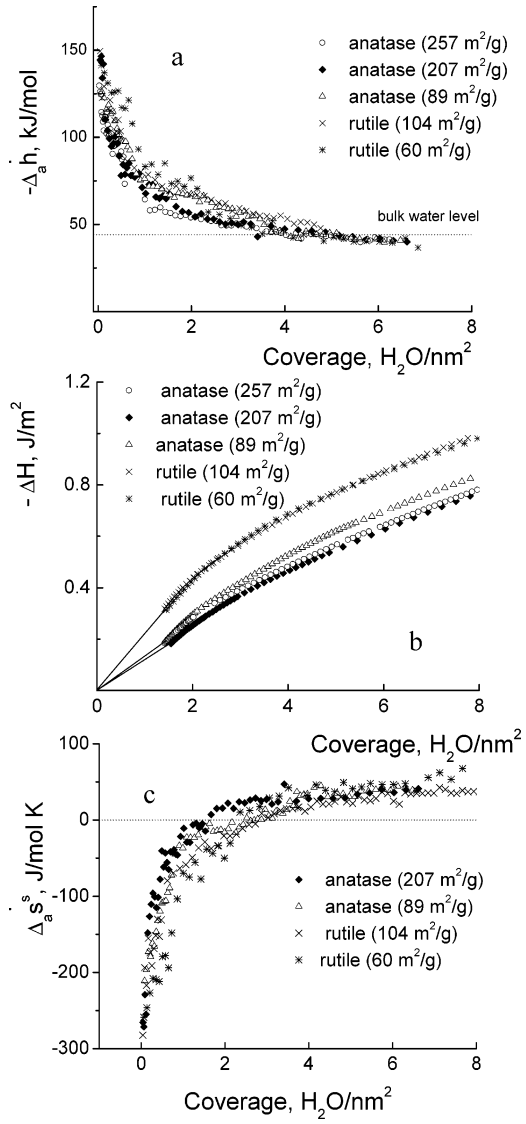

Figure 3. (a) Differential and (b) integral heats of H_2O adsorption for anatase with surface areas of 89, 207, and 257 J/m^2 and for rutile with surface areas of 60 and 104 J/m^2. (c) Differential entropies of H_2O adsorption for anatase and rutile relative to ice at 298 K.

rutile and anatase, respectively. As a result, the extrapolated integral heats intersect the origin. These values reflect different water binding energetics on the TiO_2 surface. The strongly bound water amounts to a similar average coverage of ~6.8 H_2O/nm^2 for anatase and rutile and constitutes a monolayer coverage by definition. The surface area occupied by a water molecule is then 0.15 nm^2. This is consistent with the average H_2O cross-section values, reported to be within the range of 0.11−.20 nm^2, with most values clustering around 0.16 nm^2.[30] From this value, one can calculate the water coverage for anatase from the linear fit in Figure 2 to be about one monolayer. The rutile coverage therefore is about two monolayers, implying some "loosely" bound water in the rutile samples. Note that this coverage, derived from the slope of the fit to the water content−surface area dependence, reflects the amount of H_2O in the rutile samples used for the drop solution experiments, not the coverage from the water adsorption calorimetry results. The experimental molecular cross-section depends largely on adsorption sites available on the surface. In the case of TiO_2 surfaces, these might be undercoordinated Ti and bridging O atoms. The character of H_2O adsorption (molecular or dissociative) and preferential adsorption sites are under intensive investigation in the literature both theoretically[31,32] and experimentally[20] and are beyond the scope of this study.

The integral adsorption enthalpies are −62 and −84 kJ/mol (−18 and −40 kJ/mol, respectively, in excess of the water condensation enthalpy) for anatase and rutile respectively. The error for water adsorption enthalpy is ±3 kJ/mol, as estimated on the basis of enthalpy deviations in the plateau regime, in which the water has the energetics of bulk water. The values of water adsorption enthalpy are in general agreement with previous data on TiO_2 (55−80 kJ/mol) derived by temperature-programmed desorption and immersion methods.[19,22]

As expected, the partial molar entropies relative to liquid water, calculated using eq 6, approach zero in a loosely bound water regime (not shown), with all lower-coverage data points being negative. The partial molar entropies relative to hexagonal ice derived from eq 7 are presented in Figure 3c. The first half of strongly bound water (below 2.5−3.5 H_2O/nm^2 in terms of total coverage) has negative entropy relative to ice. This negative entropy may indicate dissociation and strongly bound (immobile) OH on the TiO_2 surface.

Using eq 15, the integral entropies of adsorption for strongly bound water are calculated as −208 and −282 J mol^{-1} K^{-1} for anatase and rutile, respectively. These values are excessively negative, suggesting again strongly bound hydroxyls and the mixed (physical−dissociative) type of water adsorption.

Thermochemistry. From a thermodynamic viewpoint, the phase stability is governed by the Gibbs free energy (eq 1). Low-temperature heat capacity and entropy data reveal that rutile and anatase have the same entropy within experimental error (S^0 (298 K, rutile) = 50.6 ± 0.6 J mol^{-1} K^{-1} and S^0 (298 K, anatase) = 49.9 ± 0.3 J mol^{-1} K^{-1}).[33] The recent study by Boerio-Goates[27] has shown that, with a proper correction for adsorbed water, the entropies of nanophase TiO_2 polymorphs are similar to those of bulk materials. Thus, the $T\Delta S$ does not significantly alter the sequence of stability, and we can use enthalpies to represent the stability landscape of nanophase TiO_2.

We employ high-temperature drop solution calorimetry to derive enthalpies of formation for nanophase TiO_2 relative to the most stable bulk rutile. The measured heat effect (drop solution enthalpy, ΔH_{ds}) consists of the heat content, heat of H_2O removal, and heat of TiO_2 dissolution.

The transformation enthalpy (ΔH_{trans}) of an anhydrous material, which is the difference between formation enthal-

(30) McClellan, A. L.; Harnsberger, H. F. *J. Colloid Interface Sci.* **1967**, *23* (4), 577−99. Hall, P. G.; Langrangoldsmith, H. *J. Phys. Chem.* **1992**, *96* (2), 867−870.

(31) Zhang, C.; Lindan, P. J. D. *J. Chem. Phys.* **2003**, *119* (17), 9183−9190. Langel, W. *Surf. Sci.* **2002**, *496* (1−2), 141−150.

(32) Stefanovich, E. V.; Truong, T. N. *Chem. Phys. Lett.* **1999**, *299* (6), 623−629. Selloni, A.; Vittadini, A.; Gratzel, M. *Surf. Sci.* **1998**, *404* (1−3), 219−222.

(33) Robie, R. A.; Hemingway, B. S. *U. S. Geol. Surv. Bull.* **1995**, 2131.

pies of a given nanophase sample and bulk rutile, arises from polymorphism and surface enthalpy and can be written as

$$\Delta H_{trans}\ (\text{bulk} \rightarrow \text{nano}) = \Delta H_{trans}\ (\text{bulk rutile} \rightarrow \text{bulk anatase}) + \gamma A_{sur} = \Delta H_1 \quad (16)$$

where γ is the surface enthalpy and A_{sur} is the surface area. Note that the first term in eq 16 is zero for nanophase rutile.

For samples containing H_2O, the differences in ΔH_{ds} (ΔH_1 in the cycle below) of a nanophase sample and bulk rutile result from polymorphism, surface energy, and presence of water. The calculation of ΔH_{trans} is then carried out through the following thermochemical cycle.

$$TiO_2 \cdot wH_2O\ (\text{nano, 298 K}) \rightarrow TiO_2\ (\text{soln, 975 K}) + wH_2O\ (\text{g, 975 K})\ \Delta H_2 \quad (17)$$

$$wH_2O\ (\text{g, 975 K}) \rightarrow wH_2O\ (\text{l, 298 K})\ \Delta H_3 \quad (18)$$

$$TiO_2\ (\text{nano, 298 K}) + wH_2O\ (\text{l, 298 K}) \rightarrow TiO_2 \cdot wH_2O\ (\text{nano, 298 K})\ \Delta H_4 \quad (19)$$

$$TiO_2\ (\text{soln, 975 K}) \rightarrow TiO_2\ (\text{rutile, 298 K})\ \Delta H_5 \quad (20)$$

$$TiO_2\ (\text{rutile, 298 K}) \rightarrow TiO_2\ (\text{nano, 298 K})\ \Delta H_{trans} = \Delta H_1 \quad (21)$$

$$\Delta H_{trans} = -(\Delta H_2 + \Delta H_3 + \Delta H_4 + \Delta H_5) \quad (22)$$

The drop solution enthalpies are summarized in Table 1. Using eqs 18 and 19, the enthalpies of drop solution are corrected for the H_2O content w in nanoparticles using the results of water adsorption calorimetry. The average integral heats of H_2O adsorption for a coverage of 6.8 H_2O/nm^2 are then -0.89 and -0.68 J/m^2 on rutile and anatase, respectively. Loosely bound water above these coverages is considered to be bulk water and is accounted for by the condensation enthalpy (-44 kJ/mol[34]). The heat content of H_2O vapor between 298 and 979 K is 25.8 kJ/ mol.[34]

It is essential to note that the water content ranges from 0.5 to 9 wt %, which yields an enthalpy correction of 0.5−13 kJ/mol. Careful determination of both water content and energetics is thus of crucial importance here.

The transformation enthalpies ΔH_{trans} (kJ/mol) of nanophase samples corrected for water are presented vs surface areas (m^2/mol) in Figure 4. Linear fits give the surface enthalpies from the slopes. The bulk ΔH_{trans} is derived from the intercept. Figure 4a shows the enthalpy of nanophase rutile. A linear fit is drawn through the origin to derive the surface enthalpy of nanophase rutile as 2.22 ± 0.07 J/m^2. The uncertainty is given by the fitting program. The fits are error-weighted.

A linear fit for the anatase data in Figure 4b yields the surface enthalpy of anatase as 0.74 ± 0.04 J/m^2 and the enthalpy of phase transformation of bulk rutile to bulk anatase as 1.7 ± 0.4 kJ/mol. These uncertainties come from the statistical analysis of the fit. The transition enthalpy error propagates to 0.9 kJ/mol, using the heat of drop solution of 59.0 ± 0.8 kJ/mol for bulk rutile, which is consistent with

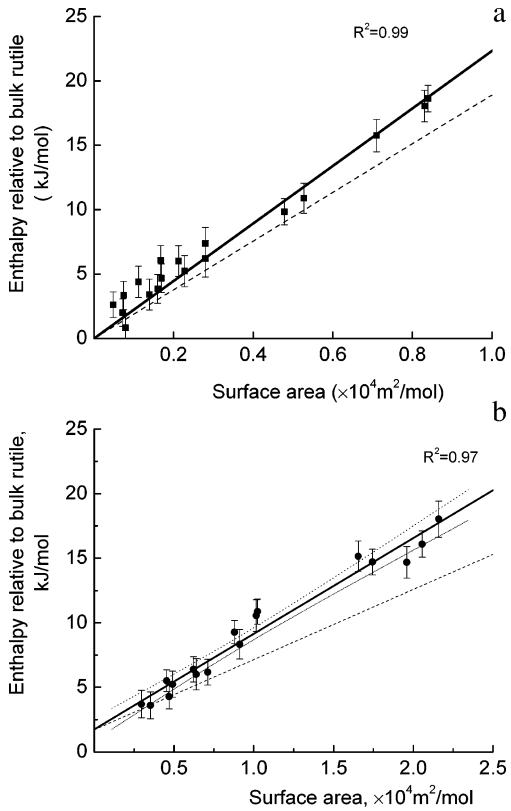

Figure 4. Formation enthalpies vs surface area for (a) rutile and (b) anatase. Solid lines are fits to the data. Dotted lines are 95% confidence bands. Dashed lines are the fits to data with bulk water correction

previous studies.[35] The recommended ΔH_{trans} value is then 1.7 ± 0.9 kJ/mol. These values are consistent with previous data by Ranade et al.[8] in that rutile has a higher surface enthalpy than anatase (Table 2). The anatase surface enthalpy is 1.85 times higher than that of Ranade[8] (0.41 ± 0.04 J/m^2) because of the bound water correction applied in our study. The fit to our data yields a surface enthalpy of 0.51 ± 0.05 J/m^2, similar to Ranada's value,[8] when the water is assumed to have the enthalpy of bulk liquid water.

The higher surface enthalpy and water adsorption energy for rutile than for anatase are consistent with the trend observed in Al_2O_3, where α-Al_2O_3 has a higher surface enthalpy (2.64 J/m^2) and a higher integral heat of H_2O adsorption (119.7 kJ/mol relative to bulk water) compared to those of γ-Al_2O_3 (1.67 J/m^2 and 78.5 kJ/mol, respectively).

Stability Landscape and Energy Crossovers. Figure 5 summarizes the energetics of three TiO_2 polymorphs. Brookite data are taken from Ranade et al.[8] The increase in metastability of the polymorph is paralleled by a decrease in surface energy, resulting in the energy crossovers seen in Figure 5. The intersections of the linear fits of brookite and rutile and of brookite and anatase show energetic stability regions. The rutile phase is energetically stable at ambient temperature for surface areas <560 m^2/mol (7 m^2/g), whereas anatase becomes stable at surface areas >4000 m^2/mol (50 m^2/g). The brookite stability region is between 560 and 4000 m^2/mol (7−50 m^2/g). The anatase and rutile energetics cross at 1100 m^2/mol (14 m^2/g). Assuming spherical particles, the

(34) *FactSage*, version 5.3; Thermfact/CRCT and GTT-Technologies: Montreal, Canada, and Aachen, Germany, 2004.

(35) Xu, H. W.; Navrotsky, A.; Nyman, M. D.; Nenoff, T. M. *J. Mater. Res.* **2000**, *15* (3), 815−823.

Table 2. Summary of Energetics for Rutile and Anatase

	sample	Ranade's data[7]	present work
surface enthalpy, J/m^2	rutile	2.2 ± 0.2^a	1.89 ± 0.08^a
		^{b}	2.22 ± 0.07^c
	anatase	0.4 ± 0.1^a	0.51 ± 0.04^a
		^{b}	0.74 ± 0.04^c
transition enthalpy, kJ/mol	bulk anatase → bulk rutile	2.61 ± 0.41^d	1.7 ± 0.9

[a] Bulk water correction. [b] Water adsorption was not measured. [c] Adsorption data correction. [d] Error was not propagated to account for the uncertainty in drop solution enthalpy for the bulk rutile.

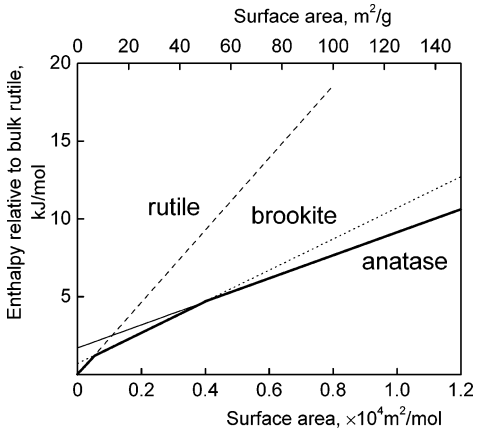

Figure 5. Energetics of nanotitania. Solid line shows energetic stability regions of different phases (brookite data from Ranade et al.[8])

calculated average diameters of rutile and brookite for 7 m^2/g surface area are about 200 nm, and of brookite and anatase for 50 m^2/g surface area are about 34 and 30 nm.

Zhang and Banfield[5,36] and Gribb and Banfield[37] studied the synthesis of fine-grained anatase and brookite and their transformation to rutile after reaching a certain particle size. They arrived at somewhat different values for the phase-stability regions of anatase and rutile: anatase became more stable than rutile for particle size <14 nm. This conclusion is somewhat uncertain, because no pure anatase in a wide range was available at the time. Moreover, the critical particle size calculation was done using surface energies from molecular modeling, rather than experimental values, and, as pointed out by Lu et al.,[38] on the basis of oversimplified assumptions that surface energy and surface stress were equal. Also, corrections for surface water were not performed. The critical size, judged by appearance of X-ray diffraction peaks, was determined from peak broadening and reflects kinetically controlled nucleation and crystal growth. Our data map the landscape of nanophase stabilities that are controlled by energetics. The wider range of nano anatase available to this study also suggests a wider window of anatase stability. For a more detailed literature analysis of previous thermodynamic data on TiO_2 energetics, we refer to the paper by Ranade et al.[8]

The calorimetric surface enthalpies for rutile and anatase are consistent with theoretical calculations based on atomistic[36] and ab initio[39,40] calculations, reporting higher surface energies for rutile relative to anatase, although the numerical values are somewhat different from our results. The theoretical methods yield energies for specific crystal faces. The relative abundance of different surfaces, even for the same area, may depend on sample preparation conditions. Our enthalpies and stability crossovers for the polymorphs in the nanophase, averaged for different crystal faces as they exist in real samples, are obtained by a direct calorimetric method with corrections made to account for surface water. The values should be reliable and representetive for real materials made by aqueous synthetic routes. Theoretical calculations of water adsorption energies on TiO_2 and other oxides show highly negative values, suggesting very negative entropies of water adsorption, in agreement with the findings of this study.[7,32,39,41]

The present study demonstrates that water plays a significant role in determining the stability of TiO_2 nanoparticles, though the interpretation is complex. The general trend of energy crossovers supports the observation that polymorphs with lower surface enthalpy are stable at the nanoscale, and thus the surface term dominates in the overall energetics. The metastable polymorph of TiO_2 (anatase) has lower surface energy and less exothermic hydration energetics, resulting in a lower level of surface hydration. The opposite is true for the most stable TiO_2 polymorph (rutile), having higher surface energy and more exothermic water adsorption energy. As suggested by the difference between surface energies for hydrated and dehydrated surfaces, the higher the water contribution to the overall free energy of the system, the more stable the hydrated surface.

The anatase nanoparticles of small surface area tend to retain the same amount of water on the surface (probably about one monolayer), observed as a linear dependence of water content vs surface area (Figure 2). The large surface area anatase has more than one hydration layer on the surface with a steeper slope for the dependence of water content on surface area. As samples coarsen, the water content becomes constant (about one monolayer). This supports the apparent two-regime character of coarsening for anatase. In the higher surface water content regime, a thick hydration layer separates nanoparticles. With surface dehydration, the particles come closer and, at some threshold, they start interacting and growing in size by aggregation. This mechanism is

(36) Zhang, H. Z.; Banfield, J. F. *J. Mater. Chem.* **1998**, *8* (9), 2073−2076.
(37) Gribb, A. A.; Banfield, J. F. *Am. Mineral.* **1997**, *82* (7−8), 717−728.
(38) Lu, H. M.; Zhang, W. X.; Jiang, Q. *Adv. Eng. Mater* **2003**, *5* (11), 787−788.
(39) Vittadini, A.; Selloni, A.; Rotzinger, F. P.; Gratzel, M. *Phys. Rev. Lett.* **1998**, *81* (14), 2954−2957.
(40) Barnard, A. S.; Zapol, P. *J. Phys. Chem. B* **2004**, *108* (48), 18435−18440. Barnard, A. S.; Zapol, P.; Curtiss, L. A. *Surf. Sci.* **2005**, *582* (1−3), 173−188.
(41) Redfern, P. C.; Zapol, P.; Curtiss, L. A.; Rajh, T.; Thurnauer, M. C. *J. Phys. Chem. B* **2003**, *107* (41), 11419−11427. Barnard, A. S.; Zapol, P.; Curtiss, L. A. *J. Chem. Theory Comput.* **2005**, *1* (1), 107−116. Lindan, P. J. D.; Harrison, N. M.; Gillan, M. J. *Phys. Rev. Lett.* **1998**, *80* (4), 762−765. Bates, S. P.; Kresse, G.; Gillan, M. J. *Surf. Sci.* **1998**, *409* (2), 336−349.

Table 3. Thermodynamic Cycle for Calculation of Entropy of Adsorbed Water at 298 K Relative to Liquid Water

$n\mathrm{TiO_2} + \mathrm{H_2O}$ (g, 298, p) → $n\mathrm{TiO_2}$·$\mathrm{H_2O}$ (adsorbed, 298, p)[a]	$\Delta_a \dot{s}$	A1
$n\mathrm{TiO_2} + \mathrm{H_2O}$ (l, 298, p) → $n\mathrm{TiO_2}$·$\mathrm{H_2O}$ (adsorbed, 298, p)	$\Delta_a \dot{s}^{\mathrm{l}} \cong \dot{s}_a - s^{\mathrm{l}}$ [b]	A2
$\mathrm{H_2O}$ (g, 298, p) → $\mathrm{H_2O}$ (l, 298, p)	$s^{\mathrm{l}} - s^{\mathrm{g}}$	A3
$\mathrm{H_2O}$ (g, 298, p) → $\mathrm{H_2O}$ (g, 298, p_0)	$R \ln p/p^0$	A4
$\mathrm{H_2O}$ (g, 298, p_0) → $\mathrm{H_2O}$ (l, 298, p_0)	$s^{\mathrm{g},0} - s^{\mathrm{l},0} = -\Delta_{\mathrm{evp}} s^0$	A5
$\mathrm{H_2O}$ (l, 298, p_0) → $\mathrm{H_2O}$ (l, 298, p)	$\cong 0$	A6
(A4) + (A5) +(A6) = (A3)	$R \ln p/p^0 - \Delta_{\mathrm{evp}} s^0$	A7
(A1) − (A3) = (A2)	$\dot{s}_{\mathrm{a}} - s^{\mathrm{l}} = \Delta_a \dot{s} - R \ln p/p^0 + \Delta_{\mathrm{evp}} s^0$	A8

[a] The cycle is calculated per mol of $\mathrm{H_2O}$, assuming there is no excess entropy of $\mathrm{TiO_2}$ as a function of particle size. [b] The entropy change of $\mathrm{TiO_2}$ is neglected; $\Delta_{\mathrm{evp}} s^0 = 147.0$ J/mol K.

Table 4. Thermodynamic Cycle for Calculation of Entropy of Adsorbed Water at 298 K Relative to Ice

$n\mathrm{TiO_2} + \mathrm{H_2O}$ (s, 298, $p^{\mathrm{l},0}$) → $n\mathrm{TiO_2}$·$\mathrm{H_2O}$ (adsorbed, 298, p)	$\Delta_a \dot{s}^{\mathrm{s}} \cong \dot{s}_{\mathrm{a}} - s^{\mathrm{i}}$	A9
$\mathrm{H_2O}$ (s, 298, $p^{\mathrm{l},0}$) → $\mathrm{H_2O}$ (g, 298, p)	Δs	A10
$\mathrm{H_2O}$ (s, 298, $p^{\mathrm{l},0}$) → $\mathrm{H_2O}$ (s, 273, $p^{\mathrm{s},0}$)	$-\int_{273}^{298} c_{\mathrm{p}}^{\mathrm{i}}\, dT/T \approx -3.4$ J mol^{-1} K^{-1}	A11
$\mathrm{H_2O}$ (s, 273, $p^{\mathrm{s},0}$) → $\mathrm{H_2O}$ (l, 273, $p^{\mathrm{l},0}$)	$\Delta_{\mathrm{m}} h/T = 22.0$ J mol^{-1} K^{-1}	A12
$\mathrm{H_2O}$ (l, 273, $p^{\mathrm{l},0}$) → $\mathrm{H_2O}$ (l, 298, $p^{\mathrm{l},0}$)	$\int_{273}^{298} c_{\mathrm{p}}^{\mathrm{l}}/T\, dT \approx 6.6$ J mol^{-1} K^{-1}	A13
$\mathrm{H_2O}$ (l, 298, $p^{\mathrm{l},0}$) → $\mathrm{H_2O}$ (g, 298, $p^{\mathrm{l},0}$)	$\Delta_{\mathrm{evp}} s^0$	A14
$\mathrm{H_2O}$ (g, 298 K, $p^{\mathrm{l},0}$) → $\mathrm{H_2O}$ (g, 298, p)	$-R \ln p/p^{0,i}$	A15
(A11) + (A12) + (A13) + (A14) + (A15) = (A10)	$-R \ln p/p^{0,\mathrm{i}} + \Delta_{\mathrm{evp}} s^{0,\mathrm{i}} + \Delta_{\mathrm{m}} h/T + \int_{273}^{298} c_{\mathrm{p}}^{\mathrm{l}}/T\, dT - \int_{273}^{298} c_{\mathrm{p}}^{\mathrm{i}}\, dT/T$	A16
(A1) +(A10) = (A9)	$\dot{s}_{\mathrm{a}} - s^{\mathrm{i}} = \Delta_a \dot{h}/T - R \ln p/p^{0,\mathrm{i}} + \Delta_{\mathrm{evp}} s^{0,\mathrm{i}} + \Delta_{\mathrm{m}} h/T + \int_{273}^{298} c_{\mathrm{p}}^{\mathrm{l}}/T\, dT - \int_{273}^{298} c_{\mathrm{p}}^{\mathrm{i}}\, dT/T$	A17

confirmed by the TEM data[6] and comparison between particle sizes derived from BET surface areas and X-ray diffraction. The same might be valid for rutile, although water content data are less conclusive.

Conclusions

The use of combined drop solution calorimetry and calorimetric measurements of water adsorption on a large number of nanophase anatase and rutile in a wide variety of surface areas has allowed for the determination of the energetics of these two polymorphs at the nanoscale level. These data suggest that strongly bound water is an essential component that controls the stability of nanoparticles.

Acknowledgment. This work was supported by DOE Grant DE FG03 01ER15237. We thank Dr. Olga Trofymluk for assistance and discussion.

CM061183C